Computation of acoustic properties and design guidelines of periodic Biot-modeled foams

Dario Magliacano[a,b,*], Morvan Ouisse[a], Sergio De Rosa[b], Francesco Franco[b], Abdelkrim Khelif[a]

[a] *FEMTO-ST Institute / Dep. of Applied Mechanics, Univ. Bourgogne Franche-Comté, CNRS/UFC/ENSMM/UTBM, Besançon, 25000, France*
[b] *Dep. of Industrial Engineering, Università di Napoli "Federico II", Corso Umberto I 40, Napoli, 80138, Italy*

Abstract

This paper aims at consolidating research dealing with vibroacoustics of periodic media. The main goal of this work is to develop and to validate tools for the design of global vibroacoustic treatments based on periodic patterns, allowing passive control of acoustic paths in layered concepts. To this aim, some enhancements are introduced to the state of the art on the the study and the design of Biot-modeled foams, in order to obtain desired acoustics performances through embedded periodic inclusions. At first, the properties of the studied acoustic package, constituted by a poro-elastic 3D unit cell, is introduced. Successively, through the use of the acoustic-structure coupling that comes from the implementation of Biot model, a non-rigid inclusion test campaign is carried out by considering some solid (but still non-perfectly-rigid) inclusions in a 3D-modeled unit cell; in particular, six setups are discussed herein. Then, some design guidelines are provided in order to predict at which frequency the first performance peak appears, together with its amplitude, as functions of unit cell dimensions, airflow resistivity, tortuosity, viscous and thermal characteristic lengths, frame density, Young modulus and loss factor; conversely, it is shown also the link between the unit cell dimensions and the first performance peak amplitude as functions of the design frequency.

*Corresponding author
Email address: dario.magliacano@univ-fcomte.fr, dario.magliacano@unina.it (Dario Magliacano)

Keywords: vibroacoustics, Biot, foam, absorption coefficient, transmission loss, design guidelines

---

Nomenclature

b	viscous drag
$G(\omega)$	relaxation function
KF	bulk modulus of the fluid phase
KS	bulk modulus of the solid phase
KB	bulk modulus of the solid phase in vacuum
N	complex shear modulus of the frame
P, Q, R	elasticity coefficients
Y	complex Young modulus of the frame
η	loss factor of the frame
μ_i	ratio of the velocity of the air over the velocity of the frame for the two compressional waves
ν	Poisson's ratio of the frame
ρ_0	bulk density of the fluid phase
ρ_1	bulk density of the solid phase
ρ_a	inertial coupling term
$\widetilde{\rho_{11}}$, $\widetilde{\rho_{12}}$, $\widetilde{\rho_{22}}$	parameters depending on the nature and the geometry of the porous medium and the density of the fluid

1. Introduction

Poro-elastic media are made of a frame with saturated fluid phase, and they attenuate sound energy through viscous and thermal dissipations, which come from fluid-structure interaction [1].

Poro-elastic materials with high porosity have interesting advantages of low density, high surface area and low manufacturing costs. Open pore foams are widely used for acoustic applications in fields such as civil and industrial engineering, thanks to their capability of dissipating sound energy in a wide frequency range [2]. However, even if foams are commonly used for noise reduction, they suffer from a lack of performances at low frequencies compared to their efficiency at higher ones [3]. This difficulty is usually overcome by multi-layering [4]. Anyway, while reducing the impedance mismatch at the air-material interface, the efficiency of such devices still relies on the allowable thickness [5, 6].

A more efficient way to enhance the low frequency response of sound packages consists in embedding periodic inclusions in a poro-elastic layer [7, 8] in order to create wave interferences or resonance effects that may improve the dynamics of the system. Indeed, structural periodic design is a powerful strategy for lightweight structures achievements [9] while remaining a convenient solution for manufacturing guidelines aspects [3, 10], since periodic media exhibit proper dynamic filtering effects that can be smartly used for vibroacoustic design [11, 12, 13, 14, 15].

In the work by Groby *et al.* [7], the influence of periodic inclusions on the acoustic performances is explained by excitation of additional acoustic modes which dissipate acoustic energy. To this aim, advanced and innovative numerical tools are more and more useful [16].

Periodic poro-elastic media, generated by uniform spatial repetition of specifically designed unit cells in the 3D domain, are extensively used in noise control applications; examples include polyurethane foams, metal foams, porous asphalt, cotton, hemp synthetic fibers, jute, glass wools, which are widely used in commercial and industrial applications [17]. Over the years, these media have been studied to the aim of their optimization for acoustic performances [3, 18]. Open cell or reticulated foams are also used in heat sink, energy absorption, packaging, architecture and even multifunctional applications. Several application-specific requirements exist; for example, in mission-critical applications such as space ones, predictability is a very high priority [17].

The typical process of material choice in these fields includes the characterization of several foams, in order to identify the most suitable one. Anyway, this process is time-consuming, and a systematic design-based approach to obtain the desired macroscale performances is still lacking. In the research performed by Deshmukh *et al.* [17], some parametric analyses about unit cell geometry, porosity, airflow resistivity, tortuosity, viscous and thermal characteristic lengths are carried out using the Johnson-Champoux-Allard (JCA) model [19, 20, 21]. For what concerns the design guidelines, similar investigations are present in the relevant literaure [22]. The main difference that is proposed herein is constituted by the extension of such parametric analyses to periodic Biot-modeled poro-elastic foams; thus, in this case, also the elastic properties of the frame are considered and analyzed [1].

In this work, some novelties are introduced to the state of the art regarding the study and the design of Biot-modeled poro-elastic materials [1], in order to estimate their acoustic performances.

In Section 2, the properties of the studied acoustic package, constituted by a poro-elastic 3D unit cell, are introduced. Successively, in Section 3, a non-rigid inclusion test campaign is carried out in terms of absorption coefficient and transmission loss, highlighting the differences between the use of a perfectly rigid inclusion and a rubber inclusion (which is an attempt to simulate an almost rigid one) in three different foams. Then, in Section 4 some guidelines are provided in order to predict at which frequency the 1^{st} performance peak (related to periodicity effects: half of the wavelength = periodicity dimension) appears, together with its amplitude, as functions of the unit cell dimensions. Conversely, also the link between the unit cell dimensions and the 1^{st} performance peak amplitude as functions of the design frequency is shown.

Furthermore, some additional guidelines are provided in order to predict at which frequency the 1^{st} performance peak appears, together with its amplitude, as functions of the foam airflow resistivity, tortuosity, viscous and thermal characteristic lengths; moreover, it is shown that frame density, Young modulus and loss factor of the foam constitute less efficient parameters in order to tune the performances of an acoustic package. In Section 5 it is also shown that, even if apparently the insertion of a periodic inclusion pattern in a layer of foam always leads to an absorption coefficient performance decay for the cases of study, instead there is an actual way to improve it without necessarily exploiting the use of Helmholtz resonators.

In conclusions, as highlighted in Section 6, the results of this investigation are very promising within the field of applications of periodic poro-elastic media in acoustics.

2. Definition of the system

This section aims at introducing the properties of the system that represents the object of the present work.

The tested unit cell is constituted by a 3D-periodic cube with side dimension r =2 cm and with a 0.5 cm radius perfectly rigid cylindrical inclusion (Figure 1). For similar cases, some results are available in literature in terms of absorption coefficient [23].

The characteristics of the poro-elastic media are reported in Table 1; in addition, quantities defined in Biot model of poro-elasticity [1] are recalled in Appendix A. It should be noted that, even if for most polymeric foams the elastic properties are frequency dependent, here they are not since, during

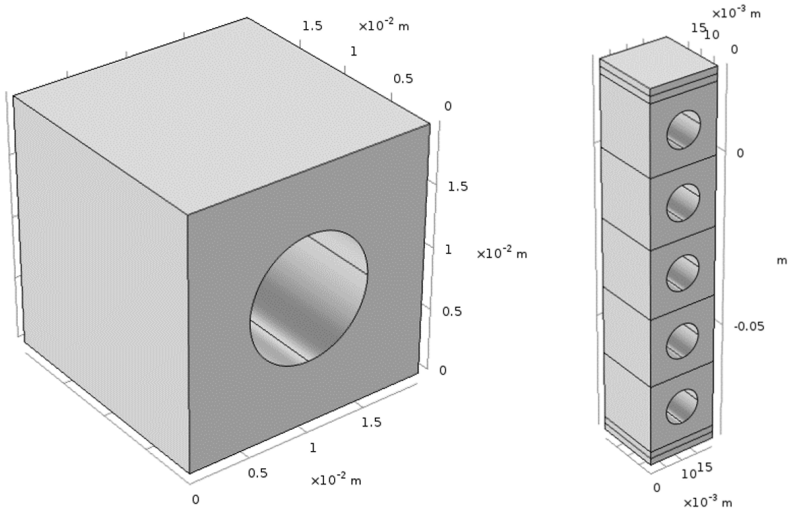

Figure 1: 3D unit cell constituted by a 2 cm cube with a 5 mm radius cylindrical hole (on the left), and a repetition of five of these unit cells (on the right).

the investigation process, it has been remarked that their frequency dependence is generally quite negligible and, in authors' opinion, does not justify the sensible increase in terms of computational time required to perform a Finite Element (FE) analysis.

The size of the cylindrical inclusion is large compared to the typical characteristic length that may be observed on a representative elementary volume describing the macroscopic behavior of the porous material [24]. The air parameters are: $\rho_{air} = 1.21 \frac{\text{kg}}{\text{m}^3}$ (density), $c_{air} = 343.3 \frac{\text{m}}{\text{s}}$ (speed of sound) and $K_{air} = 142$ kPa (bulk modulus), while the properties of the PU 60 foam are reported in Table 1.

3. Non-rigid inclusion test campaign

In this section, through the use of the acoustic-structure coupling that comes from the implementation of Biot model [1], a non-rigid inclusion test campaign that considers some solid (but still non-perfectly-rigid) inclusions in a 3D-modeled unit cell is shown, in terms of absorption coefficient and transmission loss computed at normal incidence. The general definition of the sound absorption coefficient is the fraction of incident energy propagating into a sample material versus the energy propagating out. A part of the incident energy will be absorbed into the sample material, or rather dissipated.

	PU 60	Foam 1	Foam 2
Porosity	0.98	0.96	0.97
Tortuosity	1.17	1.7	2.52
Resistivity [Pa*s/m^2]	3750	32000	87000
Viscous char. length [mm]	0.11	0.09	0.037
Thermal char. length [mm]	0.742	0.165	0.119
Density [kg/m^3]	22.1	30	31
Young modulus [kPa]	70+j19	733+j73	143+j8
Shear modulus [kPa]	25+j7	246+j26	55+j3
Loss factor	0.265	0.1	0.055
Poisson ratio	0.39	0.387	0.3

Table 1: Poro-elastic properties of the tested foams.

Since, in this case, the FE system is modeled in order to be acoustically closed, this must imply that the part of the incident propagating wave that is not reflected by the material must be absorbed, therefore the coefficient of absorption is [25]:

$$\alpha = 1 - |R|^2, \tag{1}$$

with the reflection coefficient computed from the surface impedances of the material (Z_s) and of the air (Z_0) as [25]:

$$R = \frac{Z_s - Z_0}{Z_s + Z_0}. \tag{2}$$

Transmission loss is numerically calculated as:

$$TL = 10\log_{10}\frac{\Pi_{incident}}{\Pi_{transmitted}}, \tag{3}$$

where $\Pi_{incident}$ and $\Pi_{transmitted}$ represent the incident and transmitted powers, respectively [26]. The analysis is carried out in the frequency range 0 – 9000 Hz, and classical Floquet-Bloch periodic conditions [27, 28] are used along x and y directions. The following results are related to an acoustic package composed by a finite arrangement of five unit cells (Figure 1), whose geometry and properties are described in Section 2, and the poro-elastic properties of the foams are reported in Table 1. In particular, the materials labeled as "Foam 1" and "Foam 2" indicate generic real porous materials which can easily be found on the market.

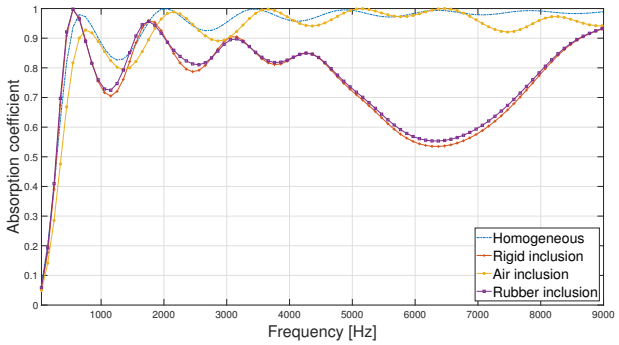

Figure 2: Non-rigid inclusion test campaign for PU 60 foam; absorption coefficient.

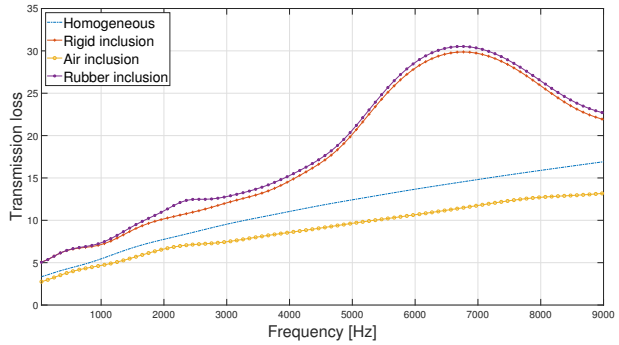

Figure 3: Non-rigid inclusion test campaign for PU 60 foam; transmission loss.

Related results are shown in Figure 2 and Figure 3. It should be noted that the mass variation related to the perfectly rigid inclusion case reported in Table 2 is negative, due to the fact that this case is purely theoretical, being representative of an inclusion with perfect sound-hard boundary walls, but with no matter inside. Additional results are provided from Figure 4 to Figure 7, obtained by carrying out the non-rigid inclusion test campaign also using Foam 1 and Foam 2, described in Table 1. Some interesting considerations may be formulated, based on the results provided herein.

In the context of the studied systems, after appropriate checks, the cause of the macroscopic resonances that are visible in the cases of PU 60 (around 6500 Hz) and Foam 1 (around 5000 Hz) has been addressed to the effect of periodicity (half of the wavelength = periodicity dimension), except from the case related to Foam 2 (around 3000 Hz), where the main visible peak is

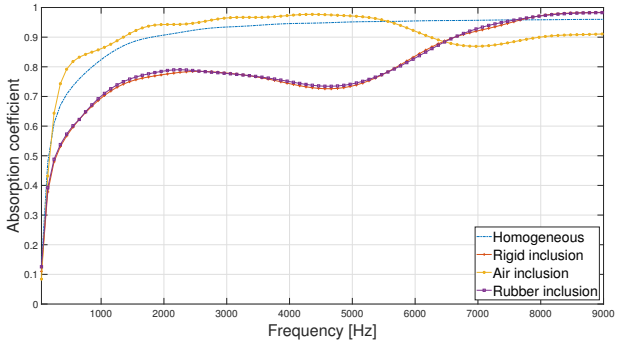

Figure 4: Non-rigid inclusion test campaign for Foam 1; absorption coefficient.

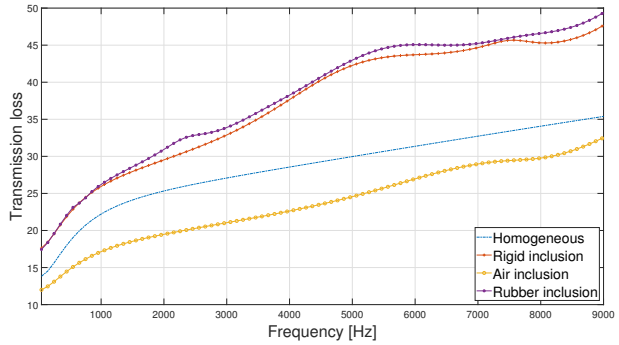

Figure 5: Non-rigid inclusion test campaign for Foam 1; transmission loss.

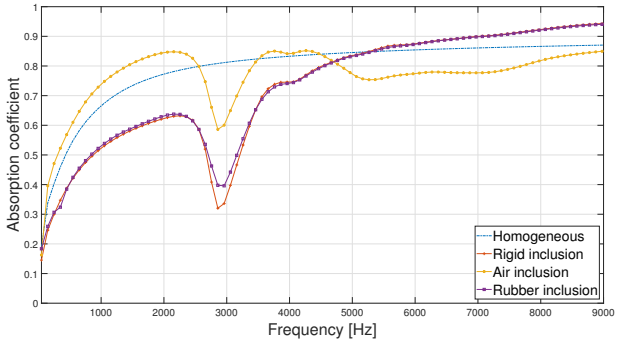

Figure 6: Non-rigid inclusion test campaign for Foam 2; absorption coefficient.

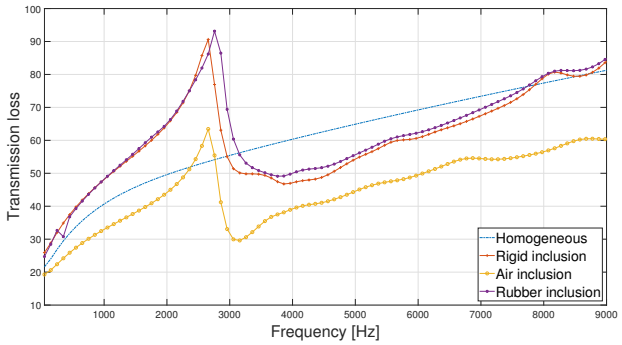

Figure 7: Non-rigid inclusion test campaign for Foam 2; transmission loss.

Configuration	**Inclusion**	**Cell mass [kg]**	**Mass variation [%]**
1	Homogeneous	$1.77 * 10^{-4}$	0
2	Perfectly rigid	$1.42 * 10^{-4}$	-19.63
3	Silicon rubber	$18.70 * 10^{-4}$	957.67

Table 2: Combinations of inclusions used in the non-rigid inclusions test campaign, with a Biot-modeled PU 60 foam, and mass variations respect to the homogeneous case.

Material	**Density [kg/m^3]**	**Young m. [kPa]**	**Poisson r.**
PU 60	22.1	70(1 + j0.265)	0.39
Silicon rubber	1100	1e6(1 + j0.4)	0.47

Table 3: Elastic properties of the materials used in the non-rigid inclusions test campaign, with a Biot-modeled PU 60 foam.

probably caused by a spring-mass effect. This is confirmed by the fact that, looking at the "Air inclusion" curves from Figure 2 to Figure 5, they do not seem to advert the effect of the inclusion, probably due to the low impedance mismatch between the contact surfaces; instead, in Figure 6 and Figure 7, the peaks are visible also in case of an inclusion filled by air, this being a further clue leading to a spring-mass resonance.

As expected, it should be noted how the sharpness of the performance peaks rises when the structural loss factor of the foam decreases. Moreover, the fact that the periodicity peak shifts backward in frequency from PU 60 case to Foam 1 case, could be explained through the higher tortuosity value of the latter. This behavior is better explained in Section 4, which provides a more detailed discussion and additional results about design guidelines.

4. Design guidelines

In this section, with reference to a PU 60 foam, some design guidelines are provided.

For some of the investigated quantities (airflow resisitivty, tortuosity, viscous and thermal characteristic lengths), some 3D plots are provided too, in which the two horizontal axes always represent the ranges of frequency and of the considered parameter, while the vertical axis shows the values of absorption coefficient (from 0 to 1) or transmission loss (from 0 dB to 100 dB).

Firstly, they are provided in order to predict at which frequency the first performance peak appears, together with its amplitude, as functions of the unit cell dimensions. Conversely, also the link between the unit cell dimensions and the first performance peak amplitude as functions of the design frequency is shown. The test campaign is carried out in the 0 – 10000 Hz frequency range, through the use of a repetition of five 3D unitary cells constituted by a 2 cm cube with a 0.5 cm radius perfectly rigid cylindrical inclusion (Figure 1), where the dimension of the inclusion changes accordingly to those of the unit cell (the ratio between the unit cell and the inclusion dimensions is kept constant).

According to the results obtained in Figure 8 and Figure 9, and considering that a typical acoustic excitation in aeronautics lays in the range of 20 – 2000 Hz [29], one should choose a unit cell dimension between 0.065 m and 0.1 m in order to obtain a transmission loss improvement of averagely 25% respect to the use of a simple foam layer of the same thickness.

Considering an automotive application, instead, the typical acoustic excita-

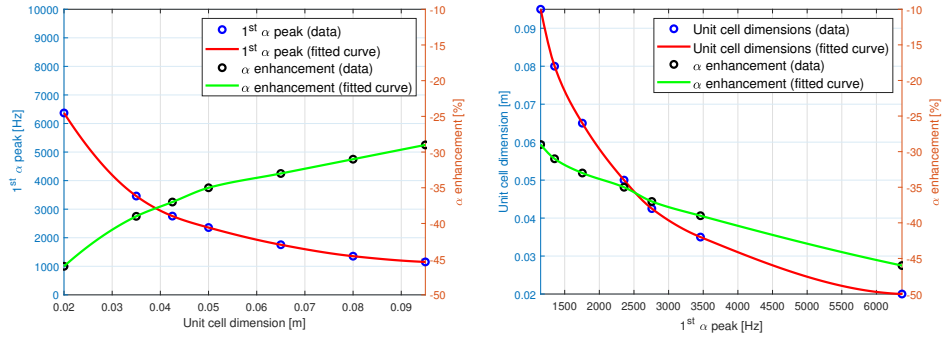

Figure 8: Absorption coefficient design curves as a function of the unit cell dimension (on the left) and the frequency of the first peak (on the right).

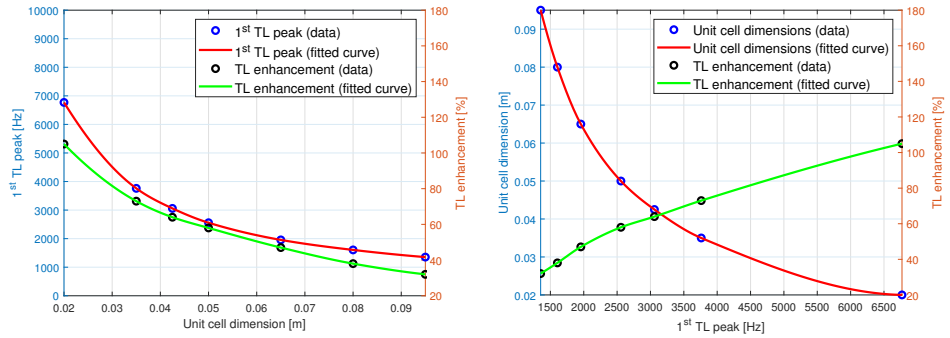

Figure 9: Transmission loss design curves as a function of the unit cell dimension (on the left) and the frequency of the first peak (on the right).

tion lays in the range of 20 – 4000 Hz [30], and therefore one should choose a unit cell dimension between 0.035 m and 0.1 m in order to obtain a transmission loss improvement of averagely 35% respect to the use of a simple foam layer of the same thickness.

Furthermore, some guidelines are also provided in order to predict at which frequency the first performance peak appears, together with its amplitude, as functions of the airflow resistivity value of the foam. The test campaign is carried out in the 0 – 10000 Hz frequency range, by comparing a repetition of five PU 60 unit cells, whose geometry is described in Figure 1 and where the airflow resistivity value is artificially changed. Looking at Figure 10, the static airflow resistivity has negligible impact on the position of the periodicity peak in the frequency range. Instead, one may notice that the

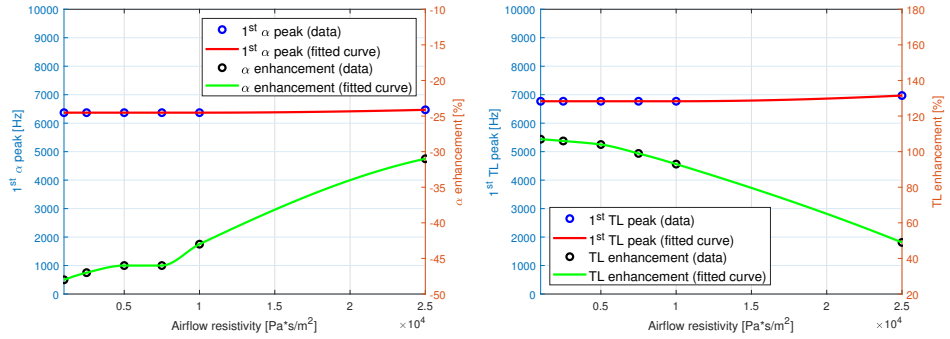

Figure 10: Absorption coefficient (on the left) and transmission loss (on the right) design curves as functions of the foam airflow resistivity.

airflow resistivity σ has a non-negligible effect on the variation of the non-homogeneous values, compared to the homogeneous ones, in correspondence of the periodicity peak. In particular, this variation reduces its amplitude at increasing airflow resistivity values, both for absorption coefficient and transmission loss performances. This is probably due to the fact that, as shown in Figure 11 and, in an even more evident manner, in Figure 12, for a homogeneous layer of foam, when σ increases absorption coefficient performances decrease, while transmission loss ones gets better. This is an expected phenomenon, since the airflow resistivity parameter may be considered as an "acoustical hardness" indicator of a foam, in the sense that, the higher it is, the less air permeability there is.

It is evident, then, that the general effect of the presence of any external inclusion in the foam reduces at increasing σ, and the non-homogeneous curves tends to assume the same behavior of the homogeneous one, still maintaining a bias difference in the average value (as it can be clearly seen from Figure 12). Indeed, already starting from $\sigma = 60000 \frac{\text{Pa*s}}{\text{m}^2}$, periodicity peaks are no more precisely identifiable.

For what concerns the tortuosity of the foam, from Figure 13 to Figure 15 it is evident that it has a strong impact on the acoustic performances of the system. In particular, at increasing tortuosity, the periodicity peak shifts backward in frequency, while also weakly reducing its amplitude.

Figure 16 show that also the viscous characteristic length has a measurable impact, in this context. The behavior is the inverse of the one related to tortuosity: at increasing viscous characteristic length, the periodicity peak shifts forward in frequency, while also weakly increasing its amplitude. In

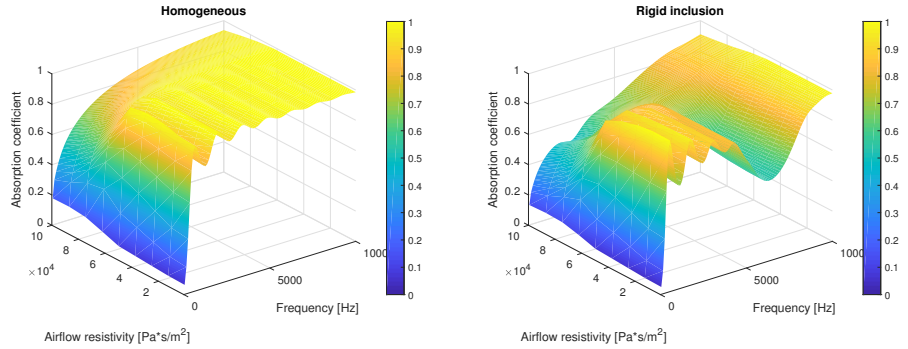

Figure 11: Absorption coefficient value as a function of frequency and foam airflow resistivity; homogeneous case (on the left) and case with a cylindrical perfectly rigid inclusion (on the right).

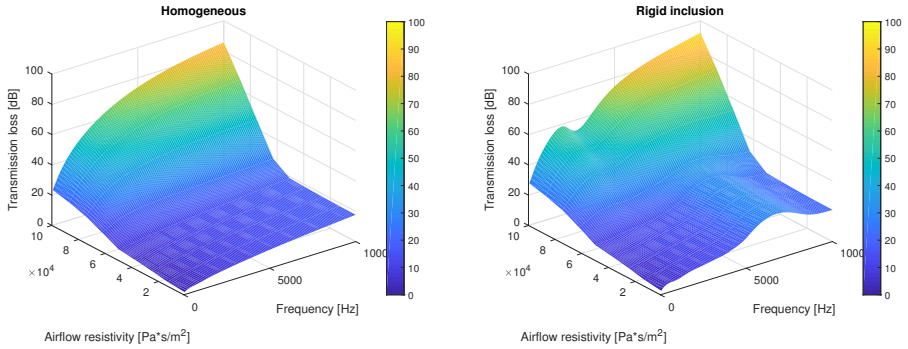

Figure 12: Transmission loss value as a function of frequency and foam airflow resistivity; homogeneous case (on the left) and case with a cylindrical perfectly rigid inclusion (on the right).

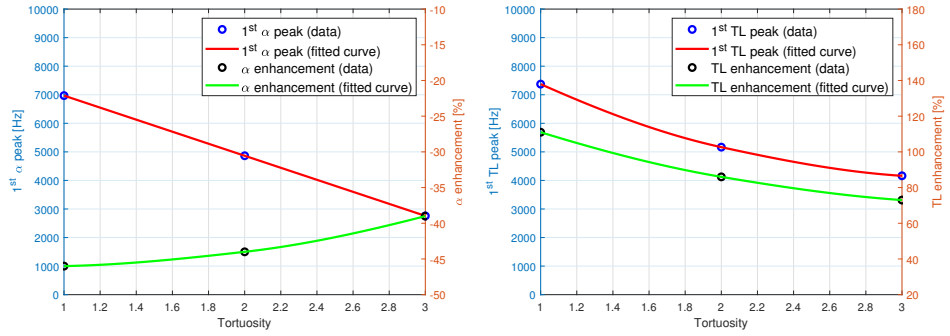

Figure 13: Absorption coefficient (on the left) and transmission loss (on the right) design curves as functions of the foam tortuosity.

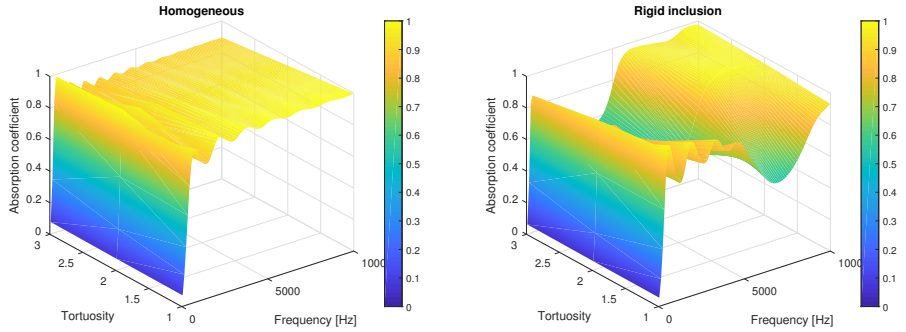

Figure 14: Absorption coefficient value as a function of frequency and foam tortuosity; homogeneous case (on the left) and case with a cylindrical perfectly rigid inclusion (on the right).

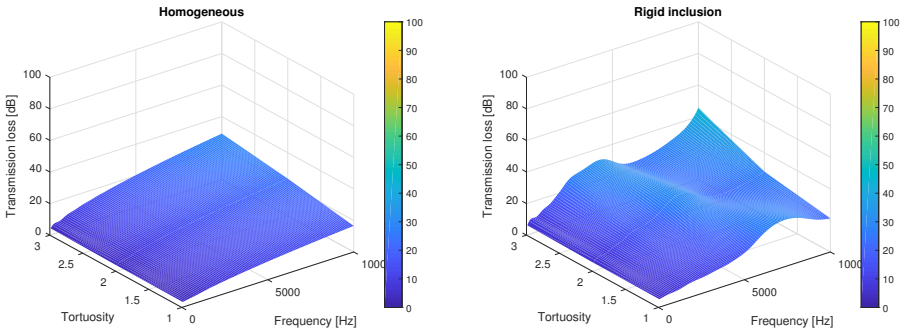

Figure 15: Transmission loss value as a function of frequency and foam tortuosity; homogeneous case (on the left) and case with a cylindrical perfectly rigid inclusion (on the right).

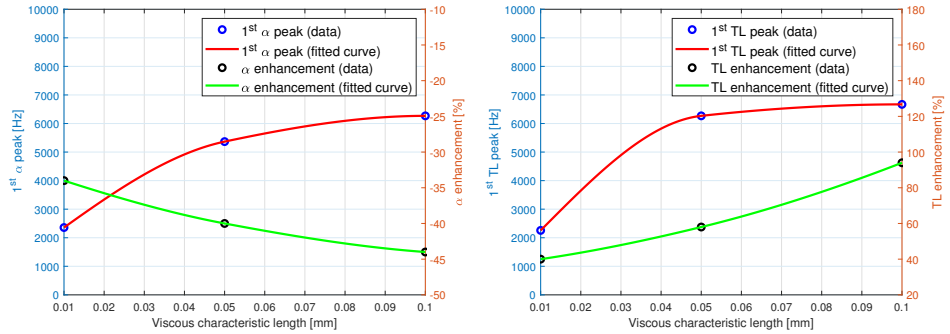

Figure 16: Absorption coefficient (on the left) and transmission loss (on the right) design curves as functions of the foam viscous characteristic length.

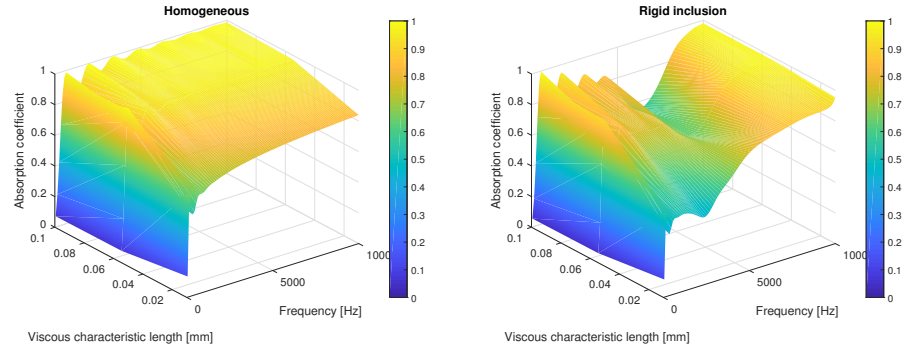

Figure 17: Absorption coefficient value as a function of frequency and foam viscous characteristic length; homogeneous case (on the left) and case with a cylindrical perfectly rigid inclusion (on the right).

addition, a higher value of viscous characteristic length means a less reflecting foam: absorption increases (Figure 17), while transmission loss decreases (Figure 18).

Differently from the viscous one, from Figure 19, Figure 17 and Figure 18 it can be stated that the thermal characteristic length has no evident impact on the frequency position of the periodicity peaks, but it has a more intense effect on their amplitude: at increasing thermal characteristic length, the periodicity peak do not shift in frequency, but increases its amplitude.

Moreover, as it can be stated from Figure 22, Figure 23 and Figure 24, frame density, Young modulus and loss factor parametric analyses do not provide any evident shifts in terms of absorption coefficient and transmission loss. Therefore it can be concluded that, for what concerns the acoustic perfor-

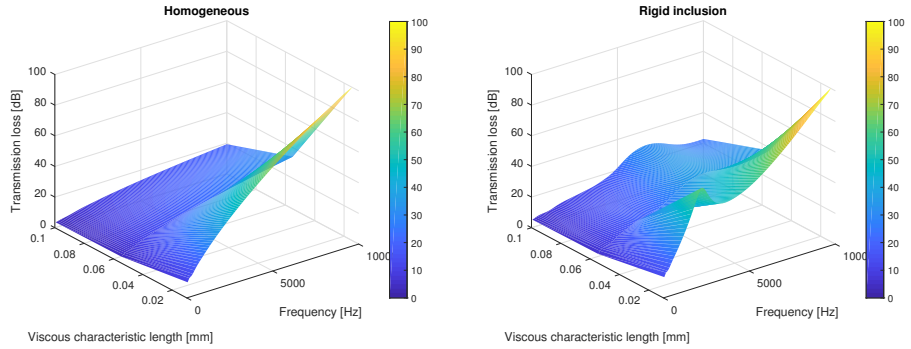

Figure 18: Transmission loss value as a function of frequency and foam viscous characteristic length; homogeneous case (on the left) and case with a cylindrical perfectly rigid inclusion (on the right).

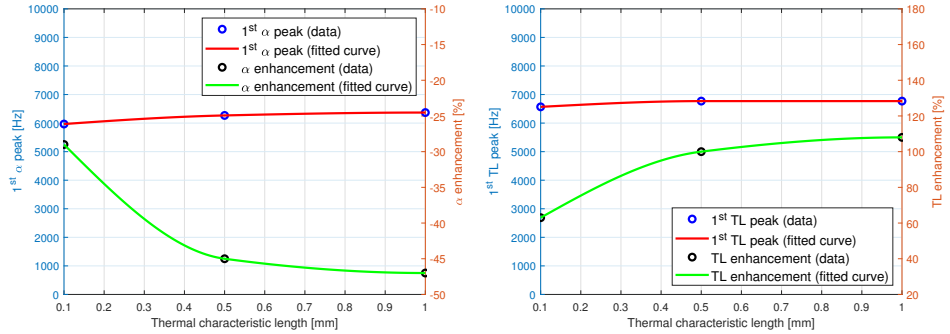

Figure 19: Absorption coefficient (on the left) and transmission loss (on the right) design curves as functions of the foam thermal characteristic length.

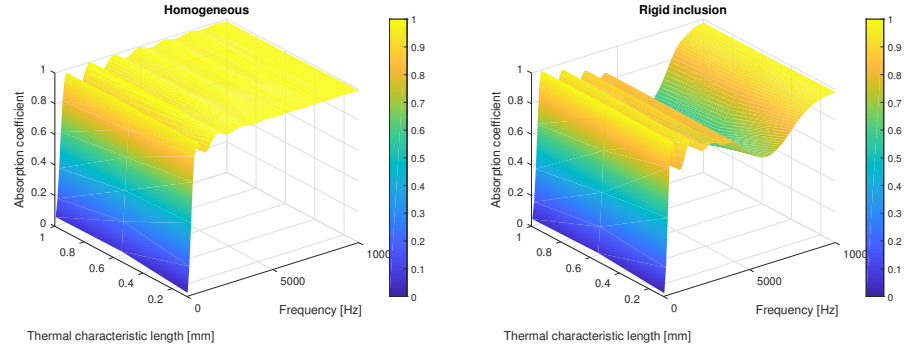

Figure 20: Absorption coefficient value as a function of frequency and foam thermal characteristic length; homogeneous case (on the left) and case with a cylindrical perfectly rigid inclusion (on the right).

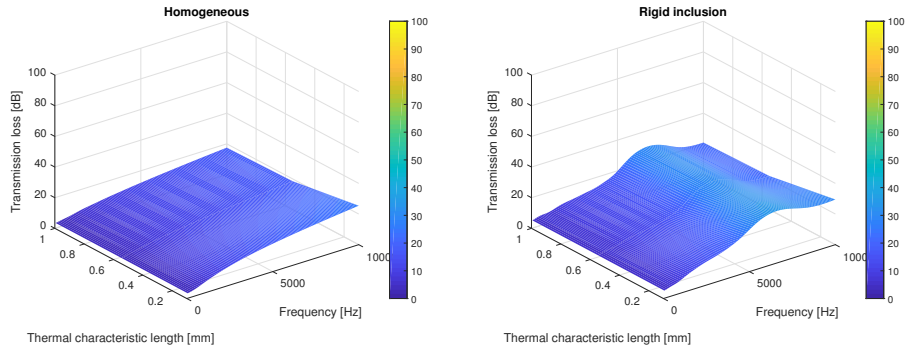

Figure 21: Transmission loss value as a function of frequency and foam thermal characteristic length; homogeneous case (on the left) and case with a cylindrical perfectly rigid inclusion (on the right).

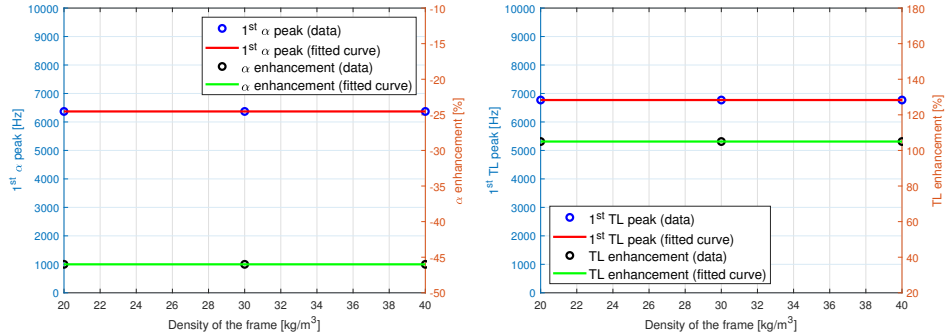

Figure 22: Absorption coefficient (on the left) and transmission loss (on the right) design curves as functions of the foam skeleton density.

mances of a periodic arrangement of unit cells, the elastic characteristics of a foam represent parameters that are less meaningful, compared to the ones related to its porous nature, in order to tune the periodicity peak. Instead, the elastic characteristics are strongly linked with the spring-mass effect, whose design guidelines are out of the scope of this work.

Summarizing, in order to tune the frequency position of an acoustic performance peak caused by periodicity effects, one should act on:

- the unit cell dimension (discordant trend),
- the tortuosity (discordant trend),
- the viscous characteristic length (concordant trend);

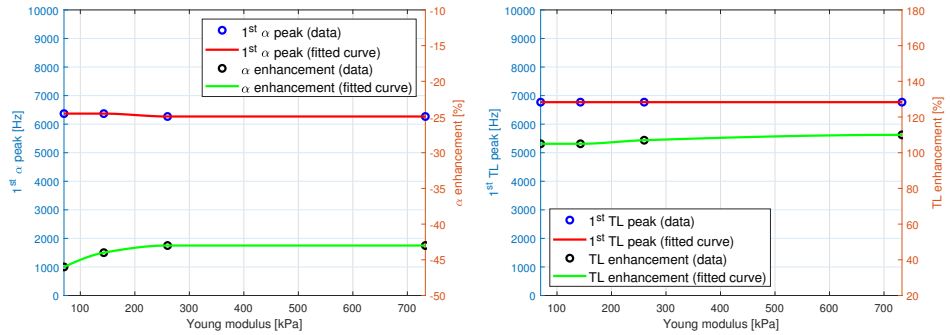

Figure 23: Absorption coefficient (on the left) and transmission loss (on the right) design curves as functions of the foam Young modulus.

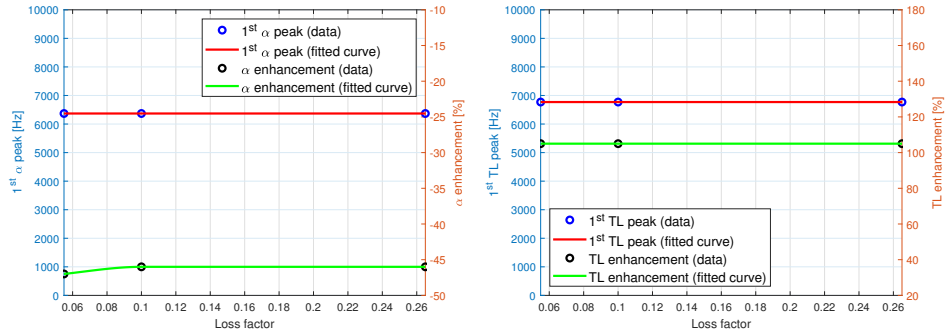

Figure 24: Absorption coefficient (on the left) and transmission loss (on the right) design curves as functions of the foam loss factor.

instead, to the aim of properly designing its amplitude, one could change:

- the unit cell dimension (discordant trend),
- the airflow resistivity (discordant trend),
- the tortuosity (discordant trend),
- the viscous characteristic length (concordant trend),
- the thermal characteristic length (concordant trend).

5. Design of absorption coefficient low frequency improvement

The aim of this section is to show that, even if apparently the insertion of a periodic inclusion pattern in a layer of foam always leads to an absorption coefficient performance decay for the cases of study (Figure 2), instead there is an actual way to improve it without necessarily exploiting the use of Helmholtz resonators [31].
If one uses a repetition of sufficiently small unit cells, some oscillations of the absorption coefficient values can be observed at low frequencies, respect to the homogeneous case. In Figure 25, the results are related to Configurations 1, 2 and 3 of Table 2, where the setup is constituted by a repetition of five 3D unit cells (Figure 1), whose side length is 0.01 m. In this situation, the differences between the perfectly rigid inclusion and the rubber inclusion cases are negligible at low frequencies. It can be noticed that the effect described above lays in the range of 550 – 1450 Hz, very interesting for acoustic applications, where the average improvement is of about 16 % .

6. Conclusions

In this work, some novelties are introduced to the state of the art regarding the study and the design of Biot-modeled poro-elastic materials, in order to estimate their acoustic performances.
First of all, the properties of the studied acoustic package, constituted by a poro-elastic 3D unit cell, have been introduced.
Then, through the use of the acoustic-structure coupling that comes from the implementation of Biot model, a non-rigid inclusion test campaign has been carried out by considering some solid (but still non-perfectly-rigid) inclusions in a 3D-modeled unit cell. In particular, six setups have been discussed.

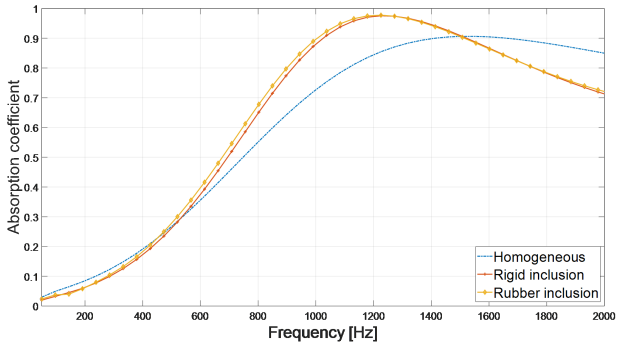

Figure 25: Absorption coefficient low frequency improvement.

Successively, some design guidelines are provided in order to predict at which frequency the first performance peak appears, together with its amplitude, as functions of unit cell dimensions, airflow resistivity, tortuosity, viscous and thermal characteristic lengths, frame density, Young modulus and loss factor; conversely, it is shown also the link between the unit cell dimensions and the first performance peak amplitude as functions of the design frequency.
The outcome of this investigation is very promising in the context of characterizations and applications of periodic poro-elastic media for aeronautic and automotive acoustic applications, and the presented results are qualitatively applicable beyond the configurations studied herein. Future works can focus on embedding resonant inclusions in a porous layer, which offer an alternative to multi-layering and double porosity materials in the design of sound absorption and insulation packages for low frequency applications.

Appendix A. Quantities defined in Biot model of poro-elasticity

- $A_1 = \omega^2 \frac{\widetilde{\rho_{11}} R - 2\widetilde{\rho_{12}} Q + \widetilde{\rho_{22}} P}{RP - Q^2}$;
- $A_2 = \omega^4 \frac{\widetilde{\rho_{11}}\widetilde{\rho_{22}} - \widetilde{\rho_{12}}^2}{RP - Q^2}$;
- $b = \sigma \phi^2 G(\omega)$;
- $G(\omega) = \sqrt{1 + \frac{4j\alpha_\infty^2 \eta_{visc} \rho_0 \omega}{(\sigma \Lambda \phi)^2}}$;
- $KS = \frac{KB}{1-\phi}$;

- $KB = \frac{2N(\nu+1)}{3(1-2\nu)}$;
- $N = |N|(1+j\eta) = \frac{Y}{2(1+\nu)}$;
- $P = \frac{(1-\phi)(1-\phi-\frac{KB}{KS})KS+\phi\frac{KBKS}{KF}}{1-\phi-\frac{KB}{KS}+\phi\frac{KS}{KF}} - \frac{2}{3}N \cong (1+\frac{\nu}{1-2\nu})2N + \frac{1-\phi^2}{\phi}KF$;
- $Q = \frac{(1-\phi-\frac{KB}{KS})\phi KS}{1-\phi-\frac{KB}{KS}+\phi\frac{KS}{KF}} \cong (1-\phi)KF$;
- $R = \frac{\phi^2 KS}{1-\phi-\frac{KB}{KS}+\phi\frac{KS}{KF}} \cong \phi KF$;
- $Y = |Y|(1+j\eta)$;
- $\widetilde{\gamma} = \phi(\frac{\widetilde{\rho_{12}}}{\widetilde{\rho_{22}}} - \frac{Q}{R})$;
- $\mu_i = \frac{P\delta_i^2 - \omega^2\widetilde{\rho_{11}}}{\omega^2\widetilde{\rho_{12}} - Q\delta_i^2}, i = 1, 2$;
- $\rho_a = \phi\rho_0(\alpha_\infty - 1)$;
- $\widetilde{\rho_{11}} = \rho_1 + \rho_a + \frac{b}{j\omega}$;
- $\widetilde{\rho_{12}} = -\rho_a - \frac{b}{j\omega}$;
- $\widetilde{\rho_{22}} = \phi\rho_0 + \rho_a + \frac{b}{j\omega}$;
- $\widetilde{\rho} = (\widetilde{\rho_{11}} - \frac{\widetilde{\rho_{12}}^2}{\widetilde{\rho_{22}}})$.

References

[1] M. Biot, Mechanics of deformation, J. Appl. Physiscs 33 (4) (1962) 1482–1498.

[2] L. Cao, Q. Fu, Y. Si, B. Ding, J. Yu, Porous materials for sound absorption, Composites Communications (2018) 25–35.

[3] J. F. Allard, N. Atalla, Propagation of sound in porous media: Modelling sound absorbing materials, 2^{nd} Edition, Wiley, 2009.

[4] Y. Yang, B. R. Mace, M. J. Kingan, Wave and finite element method for predicting sound transmission through finite multi-layered structures with fluid layers, Comput. Struct. 204 (2018) 20–30.

[5] T. Weisser, Acoustic behavior of a rigidly backed poroelastic layer with periodic resonant inclusions by a multiple scattering approach, J. Acoust. Soc. Am 139 (2) (2016) 617–629.

[6] M. Gaborit, O. Dazel, P. Göransson, A simplified model for thin acoustic screens, J. Acoust. Soc. Am. 144 (1) (1962) 76–81.

[7] J.-P. Groby, A. Wirgin, L. D. Ryck, W. Lauriks, R. P. Gilbert, Y. S. Xu, Acoustic response of a rigid-frame porous medium plate with a periodic set of inclusions, J. Acoust. Soc. Am. 126 (2) (2009) 685–693.

[8] L. Xiong, B. Nennig, Y. Aurégan, W. Bi, Sound attenuation optimization using metaporous materials tuned on exceptional points, J. Acoust. Soc. Am. 142 (4) (2017) 2288–2297.

[9] C. Boutin, Acoustics of porous media with inner resonators, J. Acoust. Soc. Am. 134 (2015) 4717–4729.

[10] G. Gosse, C. Pezerat, F. Bessac, Periodic assembly of multi-coupled parallel plates: vibration propagation and acoustic radiation, 16th International Congress on Sound and Vibration 2009 5 (2009) 3019–3026.

[11] R. Rumpler, J.-F. Deü, P. Göransson, A modal-based reduction method for sound absorbing porous materials in poro-acoustic finite element models, J. Acoust. Soc. Am. 132 (5) (2012) 3162–3179.

[12] R. Rumpler, P. Göransson, J.-F. Deü, A residue-based mode selection and sorting procedure for efficient poroelastic modeling in acoustic finite element applications, J. Acoust. Soc. Am. 134 (6) (2013) 4730–4741.

[13] Z. Liu, R. Rumpler, L. Feng, Broadband locally resonant metamaterial sandwich plate for improved noise insulation in the coincidence region, Compos. Struct. 200 (2018) 165–172.

[14] Z. Liu, R. Rumpler, L. Feng, Investigation of the sound transmission through a locally resonant metamaterial cylindrical shell in the ring frequency region, J. Appl. Phys. 125 (11) (2019).

[15] A. Khelif, P. A. Deymier, B. Djafari-Rouhani, J. O. Vasseur, L. Dobrzynski, Two-dimensional phononic crystal with tunable narrow pass band: Application to a waveguide with selective frequency, J. Appl. Phys. 94 (3) (2003) 1308–1311.

[16] D. Magliacano, M. Ouisse, A. Khelif, S. D. Rosa, F. Franco, N. Atalla, M. Collet, Computation of dispersion diagrams for periodic porous materials modeled as equivalent fluids, Mech. Syst. Signal Process. 142 (2020).

[17] S. Deshmukh, H. Ronge, S. Ramamoorthy, Design of periodic foam structures for acoustic applications: Concept, parametric study and experimental validation, Materials and Design 175 (2019).

[18] O. Doutres, M. Ouisse, N. Atalla, M. Ichchou, Impact of the irregular microgeometry of polyurethane foam on the macroscopic acoustic behavior predicted by a unit-cell model, J. Acoust. Soc. Am. 136 (4) (2014) 1666–1681.

[19] D. L. Johnson, J. Koplik, R. Dashen, Theory of dynamic permeability and tortuosity in fluid-saturated porous media, J. Fluid Mech. 176 (1) (1987) 379–402.

[20] Y. Champoux, J. F. Allard, Dynamic tortuosity and bulk modulus in air-saturated porous media, J. Appl. Phys. 70 (4) (1991) 1975–1979.

[21] M. Ouisse, M. Ichchou, S. Chedly, M. Collet, On the sensitivity analysis of porous material models, Journal of Sound and Vibration 331 (2012) 5292–5308.

[22] D. Magliacano, M. Ouisse, S. D. Rosa, F. Franco, A. Khelif, Design guidelines for the acoustic performance improvement of a periodic porous material, MEDYNA: Euro-Mediterranean Conference on Structural Dynamics and Vibroacoustics 3 (2020).

[23] J.-P. Groby, A. Duclos, O. Dazel, L. Boeckx, W. Lauriks, Absorption of a rigid frame porous layer with periodic circular inclusions backed by a periodic grating, J. Acoust. Soc. Am. 129 (5) (2011) 3035–3046.

[24] O. Robin, A. Berry, O. Doutres, N. Atalla, Measurement of the absorption coefficient of sound absorbing materials under a synthesized diffuse acoustic field, J. Acoust. Soc. Am. 136 (1) (2014) 13–19.

[25] J.-P. Groby, W. Laurik, T. E. Vigran, Total absorption peak by use of a rigid frame porous layer backed by a rigid multi-irregularities grating, J. Acoust. Soc. Am. 127 (5) (2010) 2865–2874.

[26] K. Kosałan, Calculation models for analysing the sound insulating properties of homogeneous single baffles used in vibroacoustic protection, Appl. Acoust. 146 (2019) 108–117.

[27] G. Floquet, Sur les équations différentielles linéaires à coefficients périodiques [On the linear differential equations with periodic coefficients], ann. sci. l'École norm. Supérieure 12 (2) (1881) 43.

[28] F. Bloch, Uber die quantenmechanik der elektronen in kristallgittern [On the quantum mechanics of the electrons in crystal lattices], Z. Phys. 52 (1928) 555–600.

[29] A. Peiffer, Full frequency vibro-acoustic simulation in the aeronautics industry, Proceedings of ISMA 2016 (2016).

[30] A. Mohanty, S. Fatima, An overview of automobile noise and vibration control, Noise Notes 13 (1) (2014) 43–56.

[31] J.-P. Groby, C. Lagarrigue, B. Brouard, O. Dazel, V. Tournat, B. Nennig, Enhancing the absorption properties of acoustic porous plates by periodically embedding helmholtz resonators, J. Acoust. Soc. Am. 137 (1) (2015).

List of Tables

List of Figures